ASTRONOMY & ASTROPHYSICS
SUPPLEMENT SERIES

FEBRUARY II **2000**, PAGE 73

Astron. Astrophys. Suppl. Ser. **142**, 73–79 (2000)

1.65 μm (H-band) surface photometry of galaxies

IV. observations of 170 galaxies with the Calar Alto 2.2 m telescope⋆

A. Boselli[1], G. Gavazzi[2], P. Franzetti[2], D. Pierini[3], and M. Scodeggio[4]

[1] Laboratoire d'Astronomie Spatiale, Traverse du Siphon, F-13376 Marseille Cedex 12, France
[2] Università degli Studi di Milano - Bicocca, P.zza dell'Ateneo Nuovo 1, 20126 Milano, Italy
[3] MPI für Kernphysik, Postfach 103980, D–69117 Heidelberg, Germany
[4] European Southern Observatory, Karl-Schwarzschild-Str. 2, D-85748 Garching bei München, Germany

Received October 5; accepted November 23, 1999

Abstract. We present near-infrared (H band) surface photometry of 170 galaxies, obtained in 1997 using the Calar Alto 2.2 m telescope equipped with the NICMOS3 camera MAGIC. The majority of our targets are selected among bright members of the Virgo cluster, however galaxies in the A262 and Cancer clusters and in the Coma/A1367 supercluster are also included. This data set is aimed at complementing the NIR survey in the Virgo cluster discussed in Boselli et al. (1997) and in the Coma Supercluster, presented in Papers I, II and III of this series. Magnitudes at the optical radius, total magnitudes, isophotal radii and light concentration indices are derived[1].

Key words: galaxies: fundamental parameters; galaxies: photometry; infrared: galaxies

1. Introduction

This work presents H-band (1.65 μm) observations of 170 galaxies in the regions of the Virgo cluster, of the A262 and Cancer clusters and in the Coma Supercluster obtained in 1997 with the Calar Alto 2.2 m telescope equipped with the NICMOS3 camera MAGIC. This is an accompanying paper of Paper III (Gavazzi et al. 2000a, this issue) where similar observations of 558 galaxies obtained with the TIRGO 1.5 m telescope are reported. Since most considerations are in common between the two papers, we preferred to give them in Paper III to avoid unnecessary duplications. Only data which depend on the Calar Alto instrumentation and telescope are given in full details here. The paper is organized as follows: Sect. 2 describes the studied sample, and the observations are outlined in Sect. 3. Image analysis strategies are discussed in Sect. 4. Preliminary results are given in Sect. 5 and summarized in Sect. 6.

2. Sample definition, observations and data reduction

The present paper contains the observation of 170 galaxies, primarily selected among late-type objects belonging to the Virgo cluster. Out of the 99 observed Virgo ($12^h \leq$ RA $\leq 13^h$, $0^o \leq$ dec $\leq 18^o$) galaxies, 84 belong to the Virgo Cluster Catalogue (VCC) of Binggeli et al. (1985) and 15, in the ouskirts of the cluster, were selected from the CGCG (Zwicky et al. 1961-68). These galaxies have velocities $V < 3000$ km s^{-1}, and can thus be considered bona-fide cluster members. Observations of 71 filler objects are also given, so subdivided:
20 are CGCG galaxies in the A262 cluster ($1^h43^m \leq$ RA $\leq 2^h1^m$, $34^o31' \leq$ dec $\leq 38^o33'$), 23 are CGCG objects in the Cancer cluster ($8^h11^m \leq$ RA $\leq 8^h25^m$, $20^o30' \leq$ dec $\leq 23^o$) and 28 are CGCG galaxies in the region $11^h30^m \leq$ RA $\leq 13^h30^m$, $18^o \leq$ dec $\leq 32^o$ containing the Coma supercluster, which includes the Coma and the Abell 1367 clusters and relatively isolated galaxies in the bridge between these two clusters.

By themselves these observations do not form a complete sample in any sense. However, combined with data published in Paper I (Gavazzi et al. 1996c), Paper II (Gavazzi et al. 1996b) (which were devoted to observations of disk galaxies), Paper III of this series

Send offprint requests to: A. Boselli

⋆ Based on observations taken at the Calar Alto Observatory, operated by the Max-Planck-Institut für Astronomie (Heidelberg) jointly with the Spanish National Commission for Astronomy.

[1] Tables 1 and 2 (full version) are only available in electronic form at the CDS via anonymous ftp to cdsarc.u-strasbg.fr (130.79.128.5) or via http://cdsweb.u-strasbg.fr/Abstract.html

and in Boselli et al. (1997: B97) (containing mainly measurements of Virgo galaxies taken with the Calar Alto 2.2 m telescope), the present survey contains a complete set of NIR observations as follows: out of the 646 galaxies, of both early and late-types in the CGCG ($m_{\rm p} \leq 15.7$) which are members to the Coma supercluster ($18^{\rm o} \leq \delta \leq 32^{\rm o}$; $11.5^{\rm h} \leq \alpha \leq 13.5^{\rm h}$) according to Gavazzi et al. (2000a), i.e. $5000 < V < 8000$ km s^{-1}, 625 (97%) have a NIR image available. Moreover the survey contains 221 out of 248 (89% complete) VCC galaxies brighter than $m_{\rm p} = 14.0$. Thus the giant members of the Virgo cluster (excluding VCC galaxies which are found in the background of the Virgo cluster) are sampled in a quasi-complete manner. A less complete coverage is at $m_{\rm p} \leq 16.0$: 277/587 objects were observed (47% complete). However, we have observed all but one the 88 late-type VCC galaxies selected as part of the central program of the Infrared Space Observatory (ISO) (see B97) brighter than $m_{\rm p} = 16.0$. These are objects lying either within 2 degrees of projected radial distance from M87 or in the corona between 4 and 6 degrees. Thus the H band survey contains a complete ($m_{\rm p} \leq 16.0$) sample of late-type dwarf members of the Virgo cluster, restricted however to a region smaller than the VCC.

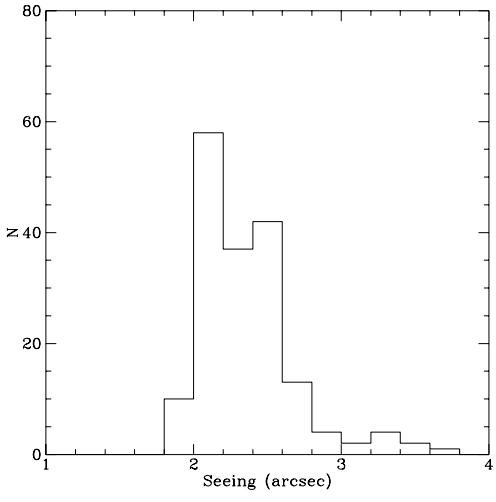

Fig. 1. The seeing distribution

2.1. Observations

The observations were carried out in three photometric nights of February 26, 27 and 28, 1997 with the Calar Alto 2.2-m telescope. The Cassegrain focus of the telescope was equipped with the MAGIC 256×256 pixel NICMOS3 infrared array (Herbst et al. 1993). In order to observe galaxies with large apparent sizes, the optical configuration of the detector was chosen to give the largest possible field of view, i.e. 6.8×6.8 arcmin^2, with a pixel size of 1.61 arcsec. The observational technique and the data reduction procedures, here just briefly summarized, are similar to the one described in B97 and in Paper III.

The seeing ranged between 2 and 3 arcsec with an average of 2.4 arcsec, as shown in Fig. 1. These seeing conditions are mostly due to the large pixels in the selected optical configuration, and as such represent a necessary disadvantage, because they also provide the large field-of-view fundamental for our observations.

At H the sky brightness (typically 13.8 mag) varied over the time scale of an observation by typically 3% in photometric conditions, by up to 8% in the worst conditions encountered. Reaching a brightness limit 8 mag arcsec^{-2} fainter than the sky requires a careful subtraction of the sky, necessitating mosaicing techniques.

As in B97 we used three types of mosaic maps, obtained by programming the telescope pointing along different patterns.

Galaxies with optical diameter larger than half of the size of the field of view of the array were observed using a mosaic in which 50% of the time is devoted to the target of interest and 50% to the surrounding sky ("A" mosaic, Fig. 2a in B97). This pattern was obtained alternating 8 fields centred on the target with 8 observations of the sky chosen along a circular path around the galaxy (off-set by a field of view from the centre). The 8 on-target fields were dithered by 10 arcsec in order to help the elimination of bad pixels.

Galaxies with optical diameter smaller than half of the size of the field of view of the array were observed with a mosaic consisting of 9 pointings along a circular path and displaced from one-another by 2 arcmin such that the target galaxy is always in the field ("B" mosaic; Fig. 2b in B97). To avoid saturation each pointing was split into 32 elementary integrations of 1 s which were added by the on-line MAGIC software. There were 7 galaxies with angular sizes larger than the dimension of the detector; these were mapped using mosaics prepared according to the shape and orientation of the galaxy in the sky in order to cover the entire surface of the target. In order to get a higher signal-to-noise two observation cycles were secured for the low surface brightness galaxies. Some galaxies were serendipitously observed in the sky frames of other targets. For these objects the number of available frames is generally ≤ 8 (see Table 1), thus their signal to noise is lower than the average value obtained for pointed galaxies.

The observations were calibrated and the fluxes transformed into the H photometric system using standard stars (Elias et al. 1982), observed hourly throughout the night. Calibration stars were observed with a third mosaic ("C", Fig. 2c in B97). This is composed of 5 pointings, starting with the target star near the centre of the array followed by pointings in each of the 4 quadrants of the

Table 1. The program galaxies. This is a one page sample. The entire table containing 170 entries is only available in electronic format

Galaxy	NGC/IC	$R.A.1950$	$Dec.$	Agg	m_p	a	b	$type$	N_f	N_c	$Seeing$	Zp	$Date$	H_{B25}	H^c_{B25}	H_T	$r_{H20.5}$	C_{31}
		$h\ m\ s$	$^\circ\ '\ ''$		mag	$arcmin$	$arcmin$				pix	$mag\ s^{-1}$	dd/mm	mag	mag	mag	$arcsec$	
(1)	(2)	(3)	(4)	(5)	(6)	(7)	(8)	(9)	(10)	(11)	(12)	(13)	(14)	(15)	(16)	(17)	(18)	(19)
VC0025	4152	120804.40	161841.0	$VCmem$	12.46	3.16	2.14	Sc	9	32	1.4	20.93	26/02	9.83	9.76	9.96	30.73	3.30
VC0058	769	120959.20	122407.0	VCM	13.17	3.16	2.19	Sb	9	32	1.7	20.99	27/02	10.38	10.31	10.51	36.46	2.79
VC0073	4180	121029.70	071900.0	VCW	13.35	2.14	0.79	Sb	9	32	1.6	20.99	27/02	9.48	9.29	9.47	40.04	3.78
VC0089	4189	121114.50	134211.0	VCM	12.53	2.82	2.04	Sc	9	32	1.8	20.99	27/02	9.30	9.24	9.31	51.87	1.79
VC0097	4193	121120.80	132703.0	VCM	13.20	2.34	1.17	Sc	9	32	1.8	20.99	27/02	9.67	9.54	9.61	52.99	2.77
VC0120	4197	121205.10	060457.0	$VCmem$	13.47	4.47	0.81	Scd	8	32	1.3	21.01	26/02	10.40	10.08	10.43	54.33	2.94
VC0145	4206	121244.00	131807.0	VCA	12.77	6.31	1.07	Sc	8	32	1.3	21.01	25/02	9.65	9.32	9.62	95.90	3.73
VC0157	4212	121306.60	141046.0	VCA	11.50	4.47	2.51	Sc	9	32	1.4	20.93	27/02	8.03	7.92	8.41	73.54	2.53
VC0167	4216	121321.50	132540.0	VCA	10.97	11.22	2.69	Sb	10	32	1.4	21.01	26/02	6.72	6.44	6.69	231.1	9.53
VC0199	4224	121400.50	074424.0	VCW	12.95	3.63	1.26	Sa	9	32	1.3	20.99	27/02	8.84	8.64	8.87	68.71	4.97
VC0222	4235	121436.70	072809.0	VCW	12.62	5.37	0.89	Sa	8	32	1.3	20.93	26/02	8.75	8.40	8.73	101.0	6.32
VC0226	4237	121438.90	153607.0	VCA	12.53	2.51	1.45	Sc	9	32	1.4	20.99	27/02	8.91	8.80	8.86	53.75	2.83
VC0234	4241	121452.60	065804.0	VCW	12.99	4.17	2.34	Sa	9	32	1.3	20.99	28/02	9.10	8.99	9.23	58.59	4.09
VC0267	3115	121526.70	065553.0	$VCmem$	13.82	2.51	2.51	Sbc	18	32	1.3	20.99	28/02	10.91	10.91	10.87	25.98	2.60
VC0307	4254	121617.00	144139.0	VCA	10.43	7.59	6.92	Sc	8	32	1.3	21.01	25/02	6.99	6.98	7.21	128.3	3.62
VC0324	–	121636.50	040758.0	VCW	14.78	1.56	1.33	BCD	18	32	1.3	20.99	28/02	11.92	11.92	11.81	16.34	2.94
VC0340	–	121648.90	061117.0	VCW'	14.43	1.31	0.51	BCD	9	32	1.3	20.99	28/02	12.30	12.30	12.32	15.90	2.82
VC0341	4260	121649.00	062234.0	VCW	12.70	4.37	2.19	Sa	9	32	1.3	20.99	28/02	8.73	8.60	8.72	71.82	4.41
VC0345	4261	121650.40	60612.0	VCW	11.31	4.90	3.63	E	9	32	1.3	20.99	28/02	7.56	7.56	7.40	86.91	5.54
VC0358	4264	121702.50	060727.0	VCW	13.80	1.75	1.21	Sa	9	32	1.3	20.99	28/02	10.17	10.10	10.14	26.58	3.73
VC0359	3153	121703.60	54031.0	$VCbac$	14.80	1.01	0.87	Sc	1	32	1.3	20.99	28/02	12.13	12.10	12.00	12.33	2.77
VC0371	4268	121713.90	053340.0	VCW	13.73	2.00	0.63	$S0$	2	32	1.3	20.99	28/02	9.80	9.80	9.81	39.11	5.47
VC0382	4273	121722.70	053713.0	VCW	12.37	2.51	1.62	Sc	9	32	1.4	20.99	28/02	9.33	9.25	9.34	49.90	3.50
VC0386	4277	121730.50	053707.0	VCW	14.47	1.75	1.10	Sa	6	32	1.4	20.99	28/02	10.64	10.55	10.80	24.27	3.44
VC0393	4276	121734.50	075807.0	VCW	13.25	2.10	2.10	Sc	9	32	1.3	20.99	27/02	10.63	10.63	10.52	30.87	2.86
VC0465	4294	121845.30	114710.0	VCA	12.62	4.90	1.55	Sc	9	32	1.4	20.93	27/02	9.75	9.53	9.85	64.27	2.83
VC0483	4298	121900.50	145301.0	VCA	12.08	4.47	2.51	Sc	8	32	1.2	21.01	26/02	8.43	8.32	8.49	84.40	3.01
VC0492	4300	121908.30	053943.0	VCW	13.76	2.69	0.89	Sa	9	32	1.5	20.99	28/02	9.65	9.44	9.65	48.59	4.35
VC0497	4302	121910.10	145230.0	VCA	12.55	8.32	2.00	Sc	8	32	1.2	21.01	26/02	8.09	7.82	8.12	167.9	3.92

array. The observations of the standard stars were obtained with a defocused telescope to avoid saturation.

The typical uncertainty on the photometric calibration is ≤ 0.05 mag.

2.2. Image analysis

The reduction of two-dimensional IR frames follows procedures identical to those reported in B97 and in Paper III. These procedures are based on the IRAF data reduction package developed by NOAO and on the SAOIMAGE and PROS packages developed at the Center for Astrophysics and on STSDAS[2].

To remove the detector response, two sets of flat-field exposures were obtained on the telescope dome with (lamp-on) and without (lamp-off) illumination with a quartz lamp. The response of the detector is then contained in the normalized frame FF = [(lamp-on) − (lamp-off)] / ⟨ (lamp-on) − (lamp-off) ⟩ (per pixel).

[2] IRAF is the Image Analysis and Reduction Facility made available to the astronomical community by the National Optical Astronomy Observatories, which are operated by AURA, Inc., under contract with the U.S. National Science Foundation. STSDAS is distributed by the Space Telescope Science Institute, which is operated by the Association of Universities for Research in Astronomy (AURA), Inc., under NASA contract NAS5–26555.

Specific reduction strategies were used for the various mosaics, according to the stability of the sky during the observations. When the sky was stable to within a few percent during the observation of a galaxy (the large majority of the observations), the 8 SKY exposures (SKY_i) were combined using a median filter to obtain $\langle SKY \rangle$ for type "A" mosaics. For type "B" mosaics $\langle SKY \rangle$ was obtained by combining the 9 frames containing target+SKY with a median filter.

The mean counts $\langle c_T \rangle_i$ and $\langle c_{sky} \rangle$ were respectively determined for the i^{th} target observation and the median sky. Individual "normalized" SKY_i frames were then produced such that $SKY_i = \langle SKY \rangle \times \langle c_T \rangle_i \ / \ \langle c_{sky} \rangle$. This removed the time variations of the sky level, but, due to the source emission, introduced an (additive) offset; this was subsequently removed (see below). Occasionally, when the average response of the detector to the sky changed by more than 3% during an observation, significant temporal variations in the spatial response of the detector to the sky became discernable. Under these circumstances, only the three sky frames closest in time to each target frame were used to determine the sky. After sky removal, each target frame (T_i) was processed to obtain a flat-field, sky subtracted, corrected frame: $T_{i,corr} = [T_i - SKY_i]/FF$.

Sky-subtracted and flat-fielded frames were then registered using field stars and combined together with a median filter. This provided a satisfactory removal of the

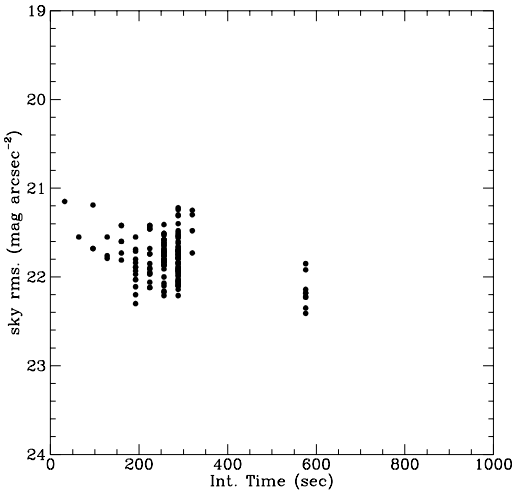

Fig. 2. The distribution of the sky rms as a function of integration time

bad pixels in the final combined image. Tests on the data showed that the photometry obtained from this use of a median filter was identical to that obtained with averaging techniques.

Star-subtracted frames were produced by a manual "editing" of the contribution from pointlike sources which are clearly not associated with the target galaxies.

The residual sky background and its rms noise (σ) (in the individual pixels) were determined in each star-subtracted frame in concentric object-free annuli around the objects of interest.

We checked the quality of the final images on large and small scales. On small scales the measured noise was always consistent with the expected statistical fluctuations in the photon count from the sky background accumulated over the total integration time. The typical pixel to pixel fluctuations are $\sim$ 22 mag arcsec^{-2}, i.e. 0.05% of the sky (see Fig. 2).

3. Results

The main results of this paper are given in Table 1 (with structure identical to Table 1 in Paper III) as follows:
Column 1: CGCG (Zwicky et al. 1961-68) or VCC (Binggeli et al. 1985) denomination.
Column 2: NGC/IC names.
Columns 3, 4: adopted (1950) celestial coordinates, measured by us or taken from NED[3], with few arcsec uncertainty.

[3] NASA-IPAC Extragalactic Databasa (NED) is operated by the Jet Propulsion Laboratory, California Institute of Technology, under contract with NASA.

Column 5: "aggregation" parameter. This parameter defines the membership to a group/cluster/supercluster: CSisol, CSpairs, CSgroups indicate members of the Coma Supercluster ($5000 < V < 8000$ km s^{-1}); CSforeg means objects in the foreground of the Coma Supercluster ($V <$ 5000 km s^{-1}) and CSbackg means objects in the background of the Coma Supercluster ($V > 8000$ km s^{-1}). Galaxies in the Virgo region are labelled following the membership criteria given by Binggeli et al. (1993): VCA, VCB, VCM, VCW, VCW′, VCSE, VCmem, are members to the cluster A or B, to the M, W, W' or South-East clouds or are not better specified members to the Virgo cluster respectively. NOVCC are galaxies taken from the CGCG in the outskirts of Virgo, but outside the area covered by the VCC. VCback are galaxies in the background of the Virgo cluster ($V > 3000$ km s^{-1}). Members to the A262 and Cancer clusters are indicated.
Column 6: photographic magnitude as given in the CGCG or in the VCC.
Columns 7, 8: for CGCG galaxies these are the major and minor optical diameters (a_{25}, b_{25}) (in arcmin) derived as explained in Gavazzi & Boselli (1996). These diameters are consistent with those given in the RC3. For VCC galaxies the diameters are measured on the du Pont plates at the faintest detectable isophote, as listed in the VCC.
Column 9: morphological type.
Column 10: number of frames $N_{\rm f}$ combined to form the final image (depending on the adopted mosaic).
Column 11: number of elementary observations (coadds) $N_{\rm c}$. The total integration time (in seconds) is the product of the number of coadds $N_{\rm c}$ times the number of combined frames $N_{\rm f}$ times the on-chip integration time $t_{\rm int}$ which was set to 1 s.
Column 12: seeing (in pixels, with 1.61 arcsec per pixel).
Column 13: adopted zero point (mag/s).
Column 14: observing date (day-month-1997).
Column 15: $H_{\rm B25}$ magnitude obtained extrapolating the present photometric measurements to the optical diameter along circular apertures as in Gavazzi & Boselli (1996).
Column 16: $H^{\rm c}_{\rm B25}$ magnitude computed at the optical diameter (see Col. 15) corrected for galactic and internal extinction following Gavazzi & Boselli (1996). The adopted internal extinction correction is $\Delta m = -2.5\,D\,\log(b/a)$ where $D = 0.17$, as determined in Boselli & Gavazzi (1994).
Column 17: $H_{\rm T}$ total H magnitude extrapolated to infinity (see Paper V, Gavazzi et al. 2000b).
Column 18: galaxy observed major ($r_H(20.5)$) radius (in arcsec) determined in the elliptical azimuthally–integrated profiles as the radii at which the surface brightness reaches 20.5 H–mag arcsec^{-2}. Galaxies which require an extrapolation larger than 0.5 mag to reach the 20.5$^{\rm th}$ magnitude isophote are labelled -1.
Column 19: the model–independent concentration index

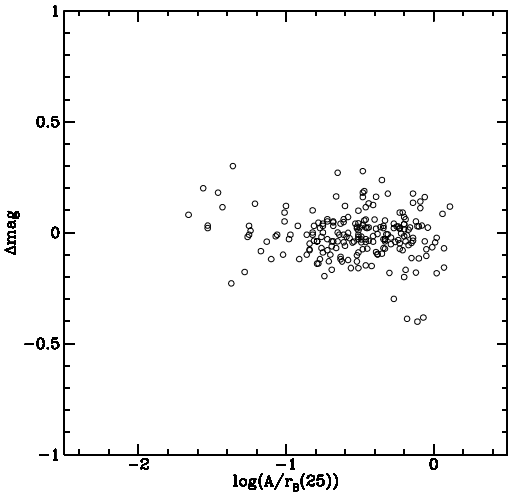

Fig. 3. The comparison between the present photometric measurements and those available from the literature as a function of the normalized aperture

C_{31} as defined in de Vaucouleurs (1977) is the ratio between the radii that enclose 75% and 25% of the total light H_T.

3.1. The virtual aperture photometry

The present data were compared with aperture photometry available in the literature by integrating the counts in concentric circular rings around the galaxy centres to provide curves of growth up to the diameter of the reference photometry. This comparison provided a general check of the intrinsic photometric accuracy of the current work. The virtual photometry measurements obtained in this work are compared with the aperture photometry available in the literature (200 measurements) in Fig. 3: on the average we find:
$H_{\rm this\ work} - H_{\rm literature} = -0.013 \pm 0.107$ mag.
A conservative estimate of the overall photometric accuracy of our data, including systematic errors on the zero point, is thus ≤ 0.1 mag.

The measurements taken through the individual "virtual circular apertures" are given in Table 2 (available only in digital format) as follows:
Column 1: Galaxy denomination in the CGCG (Z) or VCC catalogues.
Column 2: aperture diameter in arcsec.
Column 3: logarithmic ratio of the adopted aperture diameter to the optical a_{25} diameter.
Column 4: integrated H magnitude within the aperture.

Table 2. The "virtual aperture photometry". This is a one page sample. The entire table containing 2646 entries is only available in electronic format

Galaxy	*Ap.* arcsec	logAp/a_{25}	H mag
(1)	(2)	(3)	(4)
VCC 25	19.00	−1.00	10.95
VCC 25	19.30	−.99	10.94
VCC 25	29.00	−.82	10.55
VCC 25	38.60	−.69	10.30
VCC 25	48.30	−.59	10.14
VCC 25	58.00	−.51	10.06
VCC 25	67.60	−.45	10.01
VCC 25	77.30	−.39	9.99
VCC 25	86.90	−.34	9.97
VCC 25	96.60	−.29	9.95
VCC 25	106.30	−.25	9.94
VCC 25	115.90	−.21	9.94
VCC 25	125.60	−.18	9.93
VCC 25	135.20	−.15	9.93
VCC 58	19.30	−.99	12.39
VCC 58	29.00	−.82	11.82
VCC 58	38.60	−.69	11.49
VCC 58	40.60	−.67	11.44
VCC 58	48.30	−.59	11.24
VCC 58	51.80	−.56	11.16
VCC 58	58.00	−.51	11.04
VCC 58	67.60	−.45	10.90
VCC 58	77.30	−.39	10.80
VCC 58	86.90	−.34	10.73
VCC 58	96.60	−.29	10.66
VCC 58	106.30	−.25	10.61
VCC 58	115.90	−.21	10.56
VCC 58	125.60	−.18	10.52
VCC 58	135.20	−.15	10.48
VCC 58	144.90	−.12	10.46
VCC 58	154.60	−.09	10.45
VCC 58	164.20	−.06	10.44
VCC 58	173.90	−.04	10.43
VCC 73	12.90	−1.00	10.60
VCC 73	19.30	−.82	10.19
VCC 73	25.80	−.70	9.95
VCC 73	27.00	−.68	9.91
VCC 73	31.60	−.61	9.81
VCC 73	32.20	−.60	9.80
VCC 73	35.10	−.56	9.76
VCC 73	38.60	−.52	9.71
VCC 73	45.10	−.45	9.64
VCC 73	51.50	−.40	9.59
VCC 73	58.00	−.35	9.55

3.2. Radii $r_H(20.5)$

The lowest surface brightness reached in each image is given as a function of the integration time in Fig. 4 (see Paper III for a more comprehensive description of the meaning of "lowest surface brightness"). Although the present observations are deeper on average than the ones obtained at TIRGO, we decided for consistency to measure the H band radii at the same isophotal radius as in Paper III: i.e. at the 20.5 mag arcsec^{-2} isophote.

The comparison between the isophotal B band radii and the infrared $r_H(20.5)$ isophotal radii determined in this work is shown in Fig. 5. The B radii are those measured on the du Pont plates at the faintest detectable

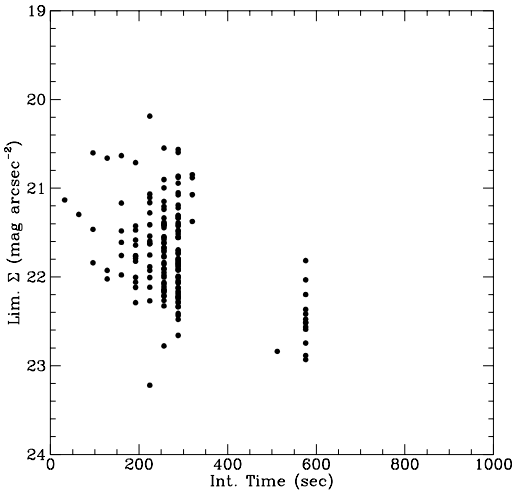

Fig. 4. The distribution of the limiting surface brightness reached in the outer light profiles, as a function of the exposure time

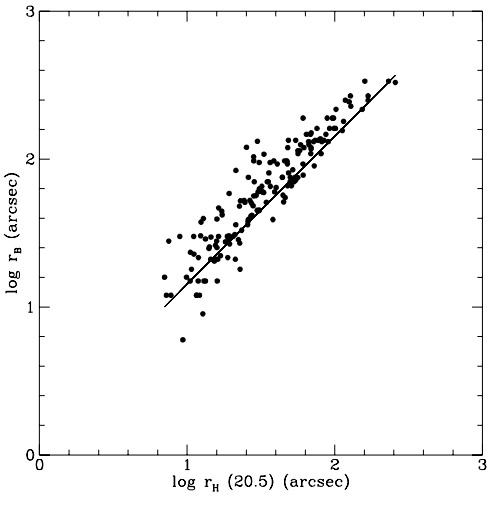

Fig. 5. The relation between the apparent major radius $r_H(20.5)$ as determined in the infrared (this work) and the optical r_B determined in the VCC at the faintest detectable isophote. The solid line represents the relation $r_H(20.5) = 0.7\ r_B(25.0)$

isophote, as listed in the VCC. These are on average larger by 25% than the standard $r_B(25.0)$ (Binggeli et al. 1985). Thus it is not surprising that the relation $r_H(20.5) = 0.7\ r_B$ used in Paper III (and reproduced as a solid line in Fig. 5) does not hold with the present data-set.

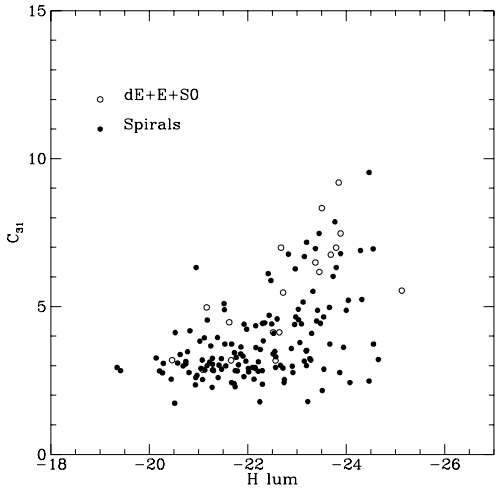

Fig. 6. The dependence of the near–infrared concentration index C_{31} on H band luminosity

3.3. Magnitudes ($H_{\rm T}$, $H_{\rm B25}$)

$H_{\rm B25}$ magnitudes listed in Col. 15 of Table 1 are obtained by extrapolating the circular aperture measurements to the optical $r_B(25.0)$ radius using standard growth curves (as in Gavazzi & Boselli 1996). [4] $H_{\rm T}$ mag instead are obtained by extrapolating to infinity the magnitude integrated along elliptical isophotes using combinations of exponential and de Vaucoulers laws (see Gavazzi et al. 2000b: Paper V). As expected, $H_{\rm T}$ are brighter than $H_{\rm B25}$ by 0.05 ± 0.15 mag on average.

3.4. Concentration index (C_{31})

The concentration index C_{31} is a measure of the shape of light profiles in galaxies, independent of a (model–dependent) bulge–disk decomposition. Values larger than ($C_{31} > 2.8$) indicate the presence of substantial bulges.

We confirm the presence in our sample of a general correlation between C_{31} and the H band (total or H_{25}) luminosity (computed from the redshift distance). We find that C_{31} generally increases toward higher absolute magnitudes (Fig. 6). High C_{31} are found only among high luminosity systems, but the reverse is not true: there are several high luminosity systems (namely late type spirals) with no or little bulge ($C_{31} \sim 3$).

4. Summary

We obtained images in the near-infrared H bandpass for an optically selected ($m_{\rm p} \leq 15.7$) sample of 170 nearby

[4] For VCC galaxies the optical radius is not determined at the 25 mag arcsec^{-2} isophote, but at the faintest detectable isophote (see Sect. 3.2).

($z < 0.02$) galaxies. As in previous papers we derive H magnitudes at the optical radius, total H magnitudes, isophotal radii at the 20.5 mag arcsec^{-2} isophote and light concentration index C_{31}. As mentioned in the Introduction, the observations presented in this paper do not cover by themselves a complete sample, but they represent the last step of our extensive NIR survey. Papers I, II, III, IV of this series and B97 contain all the data gathered so far. A comprehensive analysis of the NIR properties of galaxies will be the subject of forthcoming papers of this series. Paper V will report on the profile decomposition.

Acknowledgements. We wish to thank the Calar Alto Time Allocation Commettee for devoting three nights at the 2.2 m telescope for a project leaded by astronomers not belonging to German Institutes. We thank the MAGIC team at MPI für Astronomie for their skillful operational support and for several helpful discussions about data reduction.

References

Binggeli B., Sandage A., Tammann G., 1985, AJ 90, 1681
Binggeli B., Popescu C., Tammann G., 1993, A&AS 98, 275
Boselli A., Gavazzi G., 1994, A&A 283, 12
Boselli A., Tuffs R., Gavazzi G., Hippelein H., Pierini D., 1997, A&AS 121, 507 (B97)
de Vaucouleurs G., 1977, in: "Evolution of Galaxies and Stellar Populations", Larson R. & Tinsley B. (eds.). New Haven: Yale University Observatory, p. 43
Elias J., Frogel J., Matthews K., Neugebauer G., 1982, AJ 87, 1029
Gavazzi G., Boselli A., 1996, Ap. Lett. Comm. 35, 1
Gavazzi G., Pierini D., Boselli A., Tuffs R., 1996c, A&AS 120, 489 (Paper I)
Gavazzi G., Pierini D., Baffa C., Lisi F., Hunt L., Boselli A., 1996b, A&AS 120, 521 (Paper II)
Gavazzi G., Franzetti P., Scodeggio M., et al., 2000a, A&AS 142, 65 (Paper III)
Gavazzi G., Franzetti P., Scodeggio M., Boselli A., Pierini D., 2000b, A&AS (submitted) (Paper V)
Gezari D., Schmitz M., Pitts P., Mead J., 1993, Nasa Reference Publication, 1294
Herbst T., Beckwith S., Birk C., et al., 1993, SPIE 1946
Wainscoat R., Cowie L., 1992, AJ 103, 332
Zwicky F., Herzog E., Karpowicz M., Kowal C., Wild P., 1961-1968, "Catalogue of Galaxies and Clusters of Galaxies", Vol. 6, Pasadena, C.I.T.